Metastability of Free Cobalt and Iron Clusters: A Possible Precursor to Bulk Ferromagnetism

Xiaoshan Xu, Shuangye Yin, Ramiro Moro, Anthony Liang, John Bowlan, and Walt A. de Heer
School of Physics, Georgia Institute of Technology, Atlanta, Georgia 30332, USA
(Received 27 June 2008; published 27 July 2011)

Homonuclear cobalt and iron clusters Co_N and Fe_N measured in a cryogenic molecular beam exist in two states with distinct magnetic moments (μ), polarizabilities, and ionization potentials, indicating distinct valences. The μ is approximately quantized: $\mu_N \sim 2N\mu_B$ in the ground states and $\mu_N{}^* \sim N\mu_B$ in the excited states for Co; $\mu_N \sim 3N\mu_B$ and $\mu_N{}^* \sim N\mu_B$ for Fe. At a large size, the average μ of the two states converges to the bulk value with diminishing ionization potential differences. The experiments suggest localized ferromagnetism in the two states and that itinerant ferromagnetism emerges from their superposition.

DOI: 10.1103/PhysRevLett.107.057203 PACS numbers: 75.50.Tt, 73.22.−f, 75.75.−c

Electronic band theory explains itinerant ferromagnetism of bulk crystalline iron and cobalt in terms of a global population imbalance of partially filled electronic spin-up and spin-down bands of itinerant electrons [1]. The itinerant or localized nature of metallic ferromagnetism has been intensely debated for over a half century starting with pioneers of the quantum theory of solids coinciding with the development of band theory [1–5]. Nevertheless, ferromagnetism of iron and cobalt is still not fully understood. Following the evolution of ferromagnetism as a function of size can provide deep insight into this fundamental problem. It not only demonstrates the evolution of magnetism from isolated atoms to the bulk, but it also relates to the local magnetic order in small magnetic domains [2,3].

Previous measurements showed that the magnetic moments of cold small Co clusters and Fe clusters are enhanced: For Co_N, $\mu_N/N \approx 2\mu_B$ while for Fe_N, $\mu_N/N \approx 3\mu_B$. For larger clusters ($N > 700$) the magnetic moments converge to their respective noninteger bulk values [6–8] of $\mu_N/N \approx 1.7\mu_B$ and $2.2\mu_B$ for Co and Fe, respectively. Since surface atom spins are expected to be more localized and have increased magnetic moments, it is reasonable to attribute this convergence to the diminishing role of the surface [9–14]. However, the observed convergence is much too rapid to be explained by geometry alone [6,13,14]: For a cluster of 700 atoms, more than 40% of the atoms are on the surface; however, the moments already converge to the bulk value. Consequently, other factors must be important.

We show here that all small Fe and Co clusters exist in two states: high magnetic moment ground states (HS) and low magnetic moment excited states (LS) that are metastable. For both Co and Fe clusters, the magnetic moments $\mu_N{}^*/N$ of the LS are approximately $1\mu_B$, which is lower than the bulk value, while the magnetic moments μ_N/N of the HS are, respectively, approximately $2\mu_B$ and $3\mu_B$. We find that the HS and the LS become degenerate for a large size, while ionization potential measurements indicate that the energy gap between these two states closes with an increasing size, suggesting that the itinerant ferromagnetic state in clusters evolves from two states with different chemical valences. It is important to realize that previous experiments did not resolve these two states but rather measured an average of the two. Specifically, it is the ensemble average magnetic of the HS and the LS that rapidly converges to the bulk rather than either one of these states. This is a central observation in these experiments.

Cluster magnetic moments μ_N are determined by deflecting cold cluster beams ($20\ \mathrm{K} \leq T \leq 100\ \mathrm{K}$) in an inhomogeneous magnetic field B [6,15–17]. The magnetization M of a specific cluster is the average projection of its magnetic moment μ along the magnetic field direction, which depends on the state of the cluster. The cluster deflection δ is linearly proportional to its magnetization: $\delta = K(dB/dz)/(mv^2)M$, where m is the mass of the cluster, v is its speed, and K is a constant that depends on the geometry of the apparatus. The probability distributions of magnetizations $P(M)$ of an ensemble of clusters of a given size is determined from the shape of the deflected beam. The average magnetization $\langle M \rangle$ of this ensemble produced in a cluster source at temperature T approximately follows the Langevin function L: $\langle M \rangle = L(\mu B/k_B T)$, where k_B is the Boltzmann constant [17–19]. Hence, for each cluster size N, μ_N can be extracted from $\langle M \rangle_N$.

In brief, the experimental methods are as follows (for details, see Refs. [6,15–17,20]). A yttrium aluminum garnet laser vaporizes a small amount of metal from the sample rod located in the source. Simultaneously, a pulse of cryogenically cooled helium gas is injected into the source. The metal vapor is cooled and condenses into clusters. The clusters dwell in the cold source for about 1 ms, after which they exit the nozzle into the vacuum chamber, resulting in a beam of clusters. The cluster beam is collimated by $0.1\ \mathrm{mm} \times 5\ \mathrm{mm}$ slits. After traveling $\sim$1 m in high vacuum, the beam passes between the pole faces of a Stern-Gerlach magnet that causes the magnetic clusters to deflect. The neutral clusters enter the detector chamber, where they are photoionized with light from a

tunable pulsed laser. Positions and masses of the deflected clusters are measured with a position-sensitive time-of-flight mass spectrometer located at the end of the beam, ~2 m from the source. Beam speeds are measured by using a mechanical beam chopper. Ionization efficiencies are determined by recording the cluster ion intensities as a function of the ionization photon energy. The ionization potentials (IPs) are determined from the ionization efficiencies. Cluster polarizabilities are determined from the cluster deflections in an inhomogeneous electric field.

The probability distributions of magnetizations $P(M)$ for Co and Fe clusters are shown in Fig. 1. The magnetic moments found from Figs. 1(a) and 1(d) are consistent with previous measurements but with better precision [8]. It is known that cluster metastable states are produced in the source under certain source conditions, for example, by reducing the amount of cold helium gas injected into the source [20]. We find that this causes two component magnetic deflections for all of the clusters in the beam [Fig. 1(b)]. The deflections of the first peak correspond to the HS component and are identical to those in Fig. 1(a). The second peaks correspond to the LS component (Co_N^*). We carefully ruled out artifacts, specifically those involving bimodal operation of the source; in fact, the effect was observed in three different sources. Moreover, others seem also to have observed the effect [7]. The speed distribution of the LS clusters is identical to that of the HS clusters, indicating that the translational temperature (and the rotational temperature) is equilibrated with the source [21]. For Co_N we find that the magnetic moment and, hence, the spin

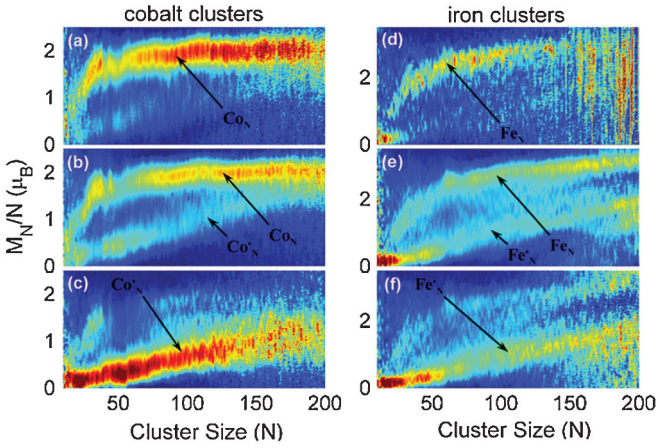

FIG. 1 (color). $P(M)$ for Co and Fe clusters for various thermalization conditions. Amplitudes are represented in color (blue: low; red: high). (a)–(c) $P(M)$ for Co clusters of 20–200 atoms under good, intermediate, and restricted thermalization conditions at $T = 20$ K and $B = 2$ T. The two branches correspond to ground state Co_N and metastable state Co_N^* clusters. The proportion of Co_N and Co_N^* can be tuned continuously, but their magnetic moments are not affected. (d)–(f) $P(M)$ for Fe clusters containing 20–200 atoms under good, intermediate, and restricted thermalization conditions at $T = 20$ K and $B = 1.2$ T, revealing two states: Fe_N with about $3\mu_B$ per atom and Fe_N^* with $1\mu_B$ per atom.

of the LS is about half of that of the ground state. The magnetic moments themselves are found not to depend on source conditions, providing further confidence in the interpretation. The LS appears for all cluster sizes, temperatures, and magnetic field ranges ($20 \le N \le 200$, $20\ \text{K} \le T \le 100\ \text{K}$, $0\ \text{T} \le B \le 2\ \text{T}$) in our experiments. Figures 1(d)–1(f) show the same effect for Fe clusters.

The following experiment confirms that the low magnetic moment states are indeed metastable. The Co cluster beam was illuminated with a pulse of 500 nm laser light before it entered the magnetic field. The $P(M)$ are compared with those without laser heating. As can be seen in Figs. 2(a)–2(c), intensity in $P(M)$ is transferred from the Co_N peak to the Co_N^* peak. Apparently, absorption of one (or at most a few) photon converts a fraction of the clusters from the HS to the LS; however, the cluster temperature (determined from the magnetization) is not significantly affected.

The IPs of the two states were derived from their ionization efficiencies. These were determined by recording the cluster ion intensity as a function of laser wavelength from 250 to 215 nm. Figure 2(d) shows the IPs for Co_N and Co_N^*. The IP difference between the HS and the LS is on

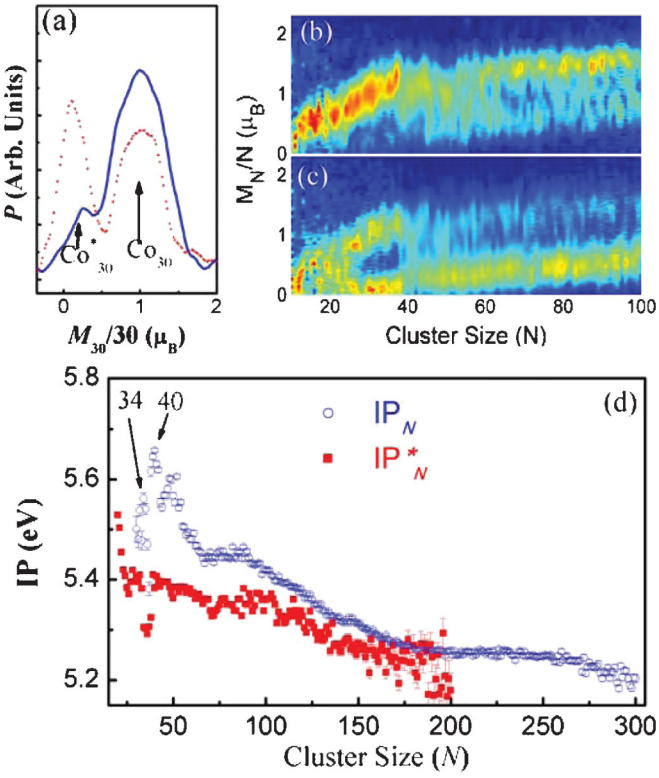

FIG. 2 (color). (a) $P(M)$ for a Co cluster of 30 atoms at 30 K. Note that when the cluster beam is heated by a 500 nm laser before it enters the magnetic field (dashed line), some of the Co_{30} are converted into Co_{30}^*. $P(M)$ of Co clusters of 10–100 atoms without (b) and with (c) laser heating are also shown. Amplitudes are represented in color (blue: low; red: high). Laser heating has the same effect as restricted thermalization. (d) Ionization potentials of Co_N(IP_N) and Co_N^*(IP_N^*).

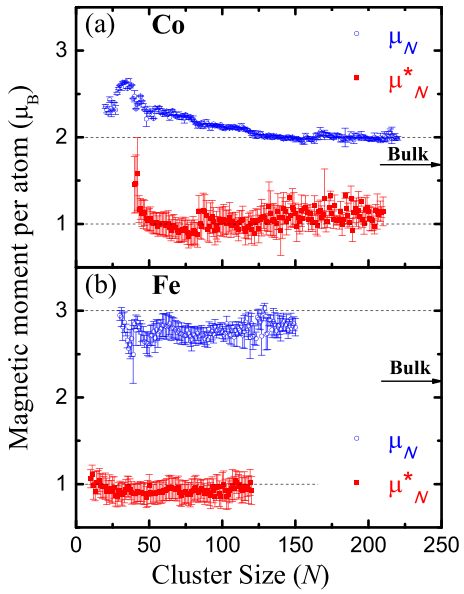

FIG. 3 (color online). Magnetic moments per atom for Co (a) and Fe (b) clusters. The magnetic moments are deduced from low field data for which, in general, $\langle M \rangle = \mu B^2/3k_BT$.

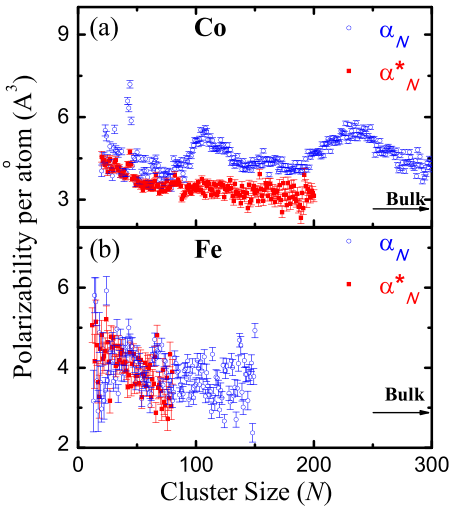

FIG. 4 (color online). Electric dipole polarizabilities of Co (a) and Fe (b) clusters.

the order of 0.1 eV for small clusters and vanishes for larger clusters ($N > 150$). Note that for Co_N, the IP_N are particularly high for $N = 34$ and $N = 40$, which suggests electronic shell effects [21].

For HS Co clusters, μ_N/N decreases slightly with increasing N and converges to about $2\mu_B$ at $N \sim 150$ [Fig. 3(a)]. For Fe_N, μ_N/N is close to $3\mu_B$ [Fig. 3(b)] for all N. The magnetic moments $\mu_N{}^*/N$ of LS Co and Fe clusters converge to $1\mu_B$ for both $Co_N{}^*$ and $Fe_N{}^*$ (Fig. 3).

The electric dipole polarizabilities of Co and Fe clusters are measured by deflecting the cluster beam in an inhomogeneous electric field [16]. For Co clusters [Fig. 4(a)], the HS polarizabilities α_N have larger values than the LS polarizabilities $\alpha_N{}^*$. The HS clusters show remarkable large undulations, whereas the LS polarizabilities decrease monotonically. For Fe clusters, α_N and $\alpha_N{}^*$ are similar [Fig. 4(b)].

The polarizability of a classical metal sphere is $R_N{}^3$, where $R_N = R_1N^{1/3}$ is the classical cluster radius. The electronic spill-out effect enhances the polarizability: $\alpha_N = (R_N + d)^3$, where d is of the order of 1 Å [22]. The $4s$ electrons are more delocalized than the $3d$ electrons so that they spill out more than the $3d$ electrons. Consequently, they are primarily responsible for the enhanced polarizabilities and for shell structure effects. Hence, the structure in the polarizabilities of Co_N and the absence of structure in $Co_N{}^*$ suggests that Co_N clusters have $4s$ electrons while $Co_N{}^*$ do not. This is also consistent with the shell structure in the IP measurements of Co_N. In contrast, the polarizabilities of Fe_N and $Fe_N{}^*$ are rather similar and featureless [Fig. 4(b)].

In summary, Co and Fe clusters exhibit two distinct magnetic states: a HS (for Co_N, $\mu_N/N \approx 2\mu_B$; for Fe_N, $\mu_N/N \approx 3\mu_B$) and a LS ($\mu^*{}_N/N \approx 1\mu_B$). For Co_N, the IP and the polarizability measurements indicate that the atomic electronic configurations of the states are different: The HS appears to have $4s$ electrons (giving rise to enhanced polarizabilities and structure in the IPs), which are absent in the LS. The energy difference between the HS and LS diminishes with increasing size.

It is clear that the clusters in either state resemble Heisenberg magnets (with ferromagnetically aligned spins localized on the atomic sites) rather than itinerant ferromagnets (with delocalized spins and noninteger moments). Accordingly, total spin in the HS is $S_{HS} = NS_1$, where $S_1 = 3/2$ for Fe and 1 for Co, and for the LS $S_{LS} = NS_2$, where $S_2 = 1/2$ for both Co and Fe. Apparently, itinerant ferromagnetism with the noninteger magnetic moments somehow evolves from these two states.

Free clusters have some similarities with supported magnetic nanostructures (i.e., magnetic atomic chains and magnetic thin films). In both cases the reduced atomic coordination decreases the interatomic overlap of electronic, thereby localizing valence electronics and enhancing the magnetic moments [6–8,23]. The absence of translational symmetry in free clusters further localizes, in particular, the $3d$ electrons [24], whose bandwidth is already narrow in the bulk limit. In contrast, the $4s$ electrons are delocalized (with a corresponding large bandwidth) and they are not spin polarized. Since the Co and Fe atomic $3d$ electrons are localized, they obey Hund's rules. However, in contrast to atoms, the orbital angular momentum is quenched (since spherical symmetry is broken), and the magnetic moments result only from electronic spins. Consequently, ferromagnetism is Heisenberg-like [5] rather than Stoner-like [1], which explains the observed integer magnetic moment per atom in the ground state. Specifically, the observed ground state magnetic moments indicate an atomic spin state (considering only the atomic d electrons) $S = 3/2$ for Fe_N and $S = 1$ for Co clusters.

This corresponds with an atomic electronic orbital configuration $3d_{\uparrow}^{5}3d_{\downarrow}^{3}4s^{1}(S=1)$ [25] for ground state Co clusters to produce $2\mu_B$ per atom. For Fe_N, the ground state configuration is $3d_{\uparrow}^{5}3d_{\downarrow}^{2}4s^{2}(S=3/2)$ to produce the observed $3\mu_B$ per atom. By the same reasoning, the excited states are also Heisenberg magnets, and atomic electronic configurations are $3d_{\uparrow}^{5}3d_{\downarrow}^{4}4s^{0}(S=1/2)$ for Co_N^* and $3d_{\uparrow}^{4}3d_{\downarrow}^{3}4s^{1}(S=1/2)$ for Fe_N^*, both with $1\mu_B$ per atom.

Cluster polarizabilities are closely related to the effective radius of the cluster. Delocalized s electrons significantly increase the polarizability of clusters beyond their classical limit due to electronic spillout. Consequently, the enhanced polarizability of Co_N^* is immediately explained: Co_N has s valence electrons, while Co_N^* does not. On the other hand, Fe_N and Fe_N^* both have the same number of s electrons and also similar polarizabilities. The large disparity in the electronic configurations of the ground state and the excited state inhibits decay [22] from the latter to the former, which explains the metastability of the excited state.

Our experiments show that both Co clusters and Fe clusters of all sizes have a stable HS and a metastable LS. One might naively assume that the LS represents an excited state of the HS since thermal excitations cause spins to misalign, reducing the overall magnetic moment, but this possibility is categorically contradicted by the experiment: To reduce the magnetic moment by a factor of 2 for Co (and 3 for Fe), as would be necessary, would require precise cluster size-dependent temperatures approaching the cluster Curie temperatures ($\sim$1200 K for Co and $\sim$800 K for Fe; see Fig. 2 in Ref. [6]). In stark contrast, the temperatures (deduced from the magnetization as explained above) for both the HS and LS are close to the cluster source temperature ($\sim$ 20 K).

The metastability of the LS is a secondary effect that probably results from the significantly different electronic structures. In fact, the Falicov-Kimball model explains the metastability in such cases as well as the degeneracy of these two states as shown in more detail in Ref. [26].

The extensive literature on cluster magnetism has not described the LS. This work presents the theoretical challenge to explain the LS state, which has the following properties: (i) The LS exists for all clusters of Fe and Co; (ii) the LS-HS energy gap diminishes and ultimately vanishes with increasing cluster size; (iii) the LS and HS represent different electronic structures with magnetic moments that are approximately quantized (on a per atom basis), consistent with different valence states; (iv) the ensemble average magnetic moment of the HS and LS converge to the bulk magnetic moments for both Fe and Co. (See [26] for a suggestion.)

In conclusion, we have experimentally demonstrated that all Fe and Co clusters have a ground state and a metastable state with corresponding approximately integer per atom magnetic moments that are, respectively, higher and lower than the bulk value. The two states become energetically degenerate for sufficiently large clusters to produce an average that closely corresponds with the bulk magnetic moments of these two metals. These experiments are readily reconciled with earlier work that demonstrated a rapid convergence of the magnetic moment to noninteger bulk values. Since the two magnetic states were not resolved in those experiments, they actually demonstrated that the ensemble average magnetic moment of these two states converges to the bulk magnetic moment value. This can hardly be an accident, but it rather strongly suggests that itinerant magnetism in these metals can be seen as evolving from these two states that become degenerate, mix, and ultimately produce the bulk itinerant ferromagnetic state.

[1] E. P. Wohlfarth, Rev. Mod. Phys. **25**, 211 (1953).
[2] H. Capellmann, *Metallic Magnetism* (Springer-Verlag, Berlin, 1987).
[3] T. Moriya, J. Magn. Magn. Mater. **14**, 1 (1979).
[4] G. T. Rado, *Magnetism* (Academic, New York, 1963).
[5] W. Heisenberg, Z. Phys. **49**, 619 (1928).
[6] I. M. L. Billas, A. Chatelain, and W. A. Deheer, Science **265**, 1682 (1994).
[7] J. P. Bucher, D. C. Douglass, and L. A. Bloomfield, Phys. Rev. Lett. **66**, 3052 (1991).
[8] D. C. Douglass *et al.*, Phys. Rev. B **47**, 12 874 (1993).
[9] G. M. Pastor, J. Dorantes-Davila, and K. H. Bennemann, Phys. Rev. B **40**, 7642 (1989).
[10] Z. Q. Li and B. L. Gu, Phys. Rev. B **47**, 13 611 (1993).
[11] M. Castro, C. Jamorski, and D. R. Salahub, Chem. Phys. Lett. **271**, 133 (1997).
[12] A. V. Postnikov, P. Entel, and J. M. Soler, Eur. Phys. J. D **25**, 261 (2003).
[13] O. Sipr, M. Kosuth, and H. Ebert, Phys. Rev. B **70**, 174423 (2004).
[14] M. L. Tiago *et al.*, Phys. Rev. Lett. **97**, 147201 (2006).
[15] W. A. Deheer and P. Milani, Rev. Sci. Instrum. **62**, 670 (1991).
[16] R. Moro *et al.*, Science **300**, 1265 (2003).
[17] X. S. Xu *et al.*, Phys. Rev. Lett. **95**, 237209 (2005).
[18] C. P. Bean and J. D. Livingston, J. Appl. Phys. **30**, S120 (1959).
[19] S. N. Khanna and S. Linderoth, Phys. Rev. Lett. **67**, 742 (1991).
[20] W. A. deHeer, P. Milani, and A. Chatelain, Phys. Rev. Lett. **65**, 488 (1990).
[21] G. Scoles, *Atomic and Molecular Beam Methods* (Oxford University, New York, 1988).
[22] W. A. Deheer, Rev. Mod. Phys. **65**, 611 (1993).
[23] F. J. Himpsel *et al.*, Adv. Phys. **47**, 511 (1998).
[24] P. W. Anderson, Phys. Rev. **109**, 1492 (1958).
[25] J. A. Alonso, Chem. Rev. **100**, 637 (2000).
[26] See Supplemental Material at http://link.aps.org/supplemental/10.1103/PhysRevLett.107.057203 for a more detailed description of the model suggested by the authors.